Journal of Materials Chemistry

Cite this: J. Mater. Chem., 2011, 21, 15175

www.rsc.org/materials

COMMUNICATION

Sculpting fabrication of nanocrater catalysts and exclusive control of wall numbers and diameters in carbon nanotubes†

Kyung Min Choi,[a] Saji Augustine,[a] Young Min Kim,[b] Ju Ho Lee,[a] Jeong Yong Lee[a] and Jeung Ku Kang*[a]

Received 11th June 2011, Accepted 5th August 2011
DOI: 10.1039/c1jm12680f

We develop the sculpting method to synthesize well-defined nanocrater catalysts with the hollow core/metal shell structure within an array *via* chemical and plasma processes. Also, we successfully demonstrate that unique morphologies of nanocrater catalysts as effective templates allow the exclusive control of the number of walls and outer diameters in carbon nanotubes.

Currently, many synthesis methods for catalytic nanoparticle using different chemical processes[1,2] have been developed, but there is still no synthesis strategy to manipulate each nanoparticle in a carved and sculpted approach. This is mostly because they rely on the pre-defined templates to control the morphology of each nanoparticle. Meanwhile, the template-free and sculpting methods could open a new generic route to the facile synthesis of many new nanoparticles not allowed in the template-based synthesis methodologies. Recent reports showed that some of the complex morphologies such as nanocups, nanocapsules, and hollow spheres could be controlled by using template-assisted processes or post-synthesis modifications.[3–5] However, crater-like nanoparticles on a substrate have not been demonstrated yet. Moreover, nanoparticle arrays with hollow interiors at a few nanometre scales are expected to provide unique and enhanced catalytic properties not expected from their bulk counterparts.[3,4] Here, we report the template-free and sculpting method that allows creation of the well-defined crater-like nanoparticle array, hereafter called the nanocrater, *via* simple but generic chemical and plasma processes. Surprisingly, this new method allows selective removal of only the core part of an individual particle such that it allows formation of homogeneous nanocrater arrays on the whole substrate. Furthermore, it is demonstrated that the nanocrater catalyst allows the exclusive fabrication of carbon nanotubes (CNTs) with a controlled number of walls without modification of their outer diameters.

In our synthesis of nanocraters, sputtered iron films (15 nm thickness) were first subjected to high temperature N_2 plasma (700 W at 800 °C) using microwave plasma enhanced chemical vapor deposition (MPCVD). Consecutively, the substrate supporting iron nanoparticles was immersed for 3.5 h in nitric acid solution for the chemical treatment. This was proven to result in formation of iron nanocraters. Then, Scanning Electron Microscopy (SEM), Atomic Force Microscopy (AFM), Transmission Electron Microscopy (TEM) and Electron Energy Loss Spectroscopy (EELS) were used for determination of their morphologies, structures, and compositions. Fig. 1 shows the structural compositional analysis for nanocrater catalysts prepared over a SiO_2 substrate. The SEM (Fig. 1b) image shows a large number of mono-dispersed iron nanocraters, where each with a uniform dark central region corresponds to the hollow interior of the nanocrater. The three-dimensional AFM image obtained from the sample in Fig. 1a confirms the crater-like hollow morphology of a nanocrater. The inverse profile (Fig. S1†) of horizontal electron intensities across one of the nanocraters in TEM

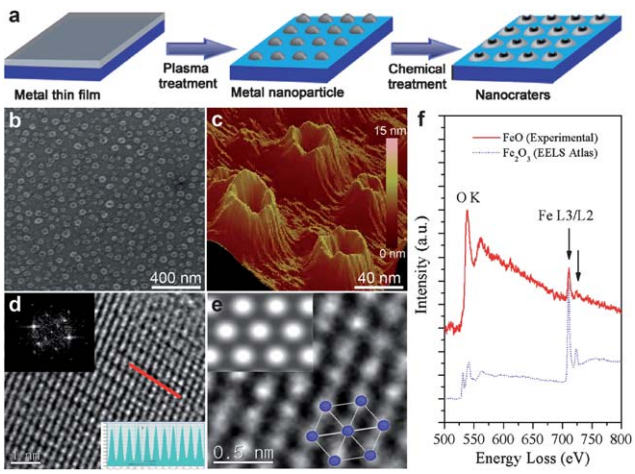

Fig. 1 Structural and compositional analysis for Fe nanocraters. (a) The schematic diagram for the nanocrater process. (b) SEM micrograph of as-synthesized Fe nanocraters on the SiO_2 substrate. (c) Three-dimensional AFM image of Fe nanocraters. (d) High-resolution image, FFT image (inset) and intensity profile (inset) for the nanocrater in (a). (e) The atomic column imaging for this sample demonstrating the defective [111] FeO structure and the calculated image (inset) with the structure information of FeO. (f) Electron energy loss spectrum for this sample.

[a]*NanoCentury & EcoEnergy KAIST Institutes, Graduate School of EEWS (WCU), Department of Materials Science & Engineering, KAIST, Daejeon, 305-701, Republic of Korea. E-mail: jeungku@kaist.ac.kr; Fax: +82-42-350-3310; Tel: +82-42-350-3338*
[b]*Division of Electron Microscopic Research, Korea Basic Science Institute, 52 Eoeun Dong, Yuseong-Gu, Deajeon, 305-806, Korea*

† Electronic supplementary information (ESI) available: Experimental procedures, detailed analysis methods, TEM plane view image and detailed analysis of Electron Energy Loss Spectroscopy. See DOI: 10.1039/c1jm12680f

analysis also supports its crater-like hollow structure. The average diameter of craters obtained from these analyses is ~40 nm and their average wall thickness is ~12 nm.

The composition of the nanocrater was analyzed by observing its cutting plane with high resolution TEM (HRTEM) and EELS, after cleaving one nanocrater. The HRTEM image (Fig. 1d) from the sample of Fig. 1a has a hexagonal symmetry because the FFT image (inset in Fig. 1d) indicates a slightly tilted [111] direction of the sample. The measured planar spacing is ~2.5 Å (see the inset intensity profile in Fig. 1d), which is in good agreement with the *d*-spacing of {111} planes for the FeO structure (JCPDS card no. 77-2355). The enlarged SAD image coincides with the [111] direction of the sample exhibiting a typical atomic structure of [111] FeO (NaCl type, space group: $Fd\bar{3}m$), as seen in Fig. 1d. In addition, we have performed multi-slice image calculation for the FeO atomic structure and compared it with the experimental image as shown in the inset of Fig. 1e. The bright columns in this image indicate Fe and O mixed columns seen in the [111] direction of the FeO structure. The hexagonal array of the bright columns in the calculated image matches with the experimental SAD image. However, the experimental FeO image is demonstrating that it is on a defective structure since the FeO phase is known to form a NaCl structure defective in Fe.[6] Also, the EELS measurement shown in Fig. 1e confirms that the chemical composition of the nanocrater consists of FeO (ESI† for more details).

We further investigate the control of size and thickness in craters with the variables of sputtered iron film thickness and chemical treatment time, respectively. The size of nanocraters was simply controlled by the metal film thickness which is determined by the sputtering time in the rf-sputter system. In this experiment, we investigate three kinds of metal film thickness (4 nm, 10 nm and 15 nm), which make different average sizes of crater nanoparticles (~17 nm, ~30 nm and ~40 nm, respectively) (Fig. 2b–d). The statistical distribution also confirms the dependence of size on the metal film thickness (Fig. 2a). The size of wall thickness in nanocraters was also controllable with the varied chemical treatment time. Three different chemical etching times (3.5 h, 4 h and 4.5 h) make different average sizes of crater nanoparticles (~10 nm, ~5.5 nm and ~4 nm, respectively), which was also verified by statistical distribution (Fig. 2e–h). This sculpting fabrication method for the nanocrater, therefore, could be extended to a wide range of dimensions for their catalytic use.

The entire process is illustrated in Fig. 3a. First, the metal thin film was deposited by sputtering onto a SiO_2 substrate. The metal films were then subjected to high temperature N_2 plasma etching using microwave plasma enhanced chemical vapor deposition (MPCVD), which forms a metal core–oxide shell structured nanoparticles (Fig. 3a and b) due to the high temperature and residual oxygen in the chamber after decomposing the film by plasma.[7] The chemical etchant of nitric acid, in the next step, selectively removes the metal core part of each nanoparticle remaining in the oxide shell part (Fig. 3a and c). This arises because metals and their amphoteric oxides have different chemical potentials when reacting with acids, particularly with an acid–base mixture.[8] Therefore, the different etching rates of the metal core to the metal oxide shell can lead to formation of crater nanoparticles. Those are also clearly shown in comparative XRD measurements (Fig. 3d); XRD peaks from Fe and FeO coexisted in metal core/oxide shell particles forming after plasma treatment, but peaks for Fe disappeared in nanocrater particles by

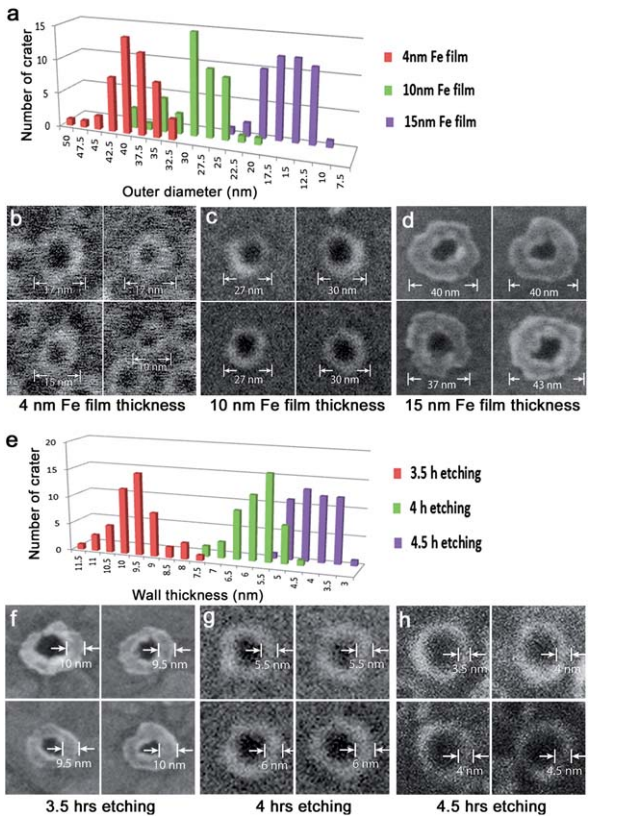

Fig. 2 The size and wall thickness control of nanocraters. (a) Statistical distribution for the nanocrater size in different metal film thicknesses. (b) 4 representative SEM images in different metal film thicknesses. (c) Statistical distribution for the wall thicknesses of nanocraters in different chemical treatment times. (d) 4 representative SEM images in different chemical treatment times.

selective etching of the metal core. Consequently, the combined method of the plasma assisted core/shell nanoparticle formation and selective etching would allow formation of nanocraters.

Also, we studied the function of nanocrater nanoparticles as catalysts to grow the CNTs having controlled structures and morphologies. The synthesis of controlled CNTs is very important in that the functionality of a CNT can be significantly tailored by

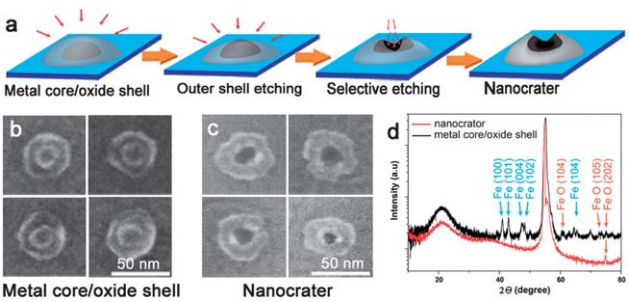

Fig. 3 The formation mechanism of the nanocrater and the core–shell structure. (a) The schematic diagram for the formation mechanism of a nanocraters. (b) SEM image for metal core/oxide shell nanoparticles after the plasma treatment. (c) SEM image for nanocrater particles after the chemical etching treatment. (d) Comparative XRD for the nanocrater and core/shell particles.

control of its diameter and the number of its walls.[9] However, the simultaneous control of the wall number and the diameter in a CNT has been a challenging issue due to their strong interdependence.[10] Interestingly, the nanocrater could be used as the host template to control the number of walls and the diameter in CNTs (Fig. 4). This arises from the fact that the CNT layer cannot be formed from its hollow core part, but only from its shell part of the nanocrater nanoparticle, while the confined size of the catalyst controls the diameter of the CNT. Under the identical synthesis conditions to grow the CNTs, the number of walls in CNTs grown from nanocrater catalysts is found to be almost half that grown from pristine catalysts in all the ranges of different diameters. The graph in Fig. 4a shows the correlation of the diameter and the thickness in the nanocrater with the diameter and the number of walls in a CNT, wherein a larger outer diameter of the nanocrater has a thicker wall, which results in the larger diameter and higher number of walls in a CNT. Fig. 4b shows representative examples in two different sizes from pristine and nanocrater catalysts. In both cases of pristine and nanocrater catalysts, typical particles with sizes of 20 nm and 38 nm were found to have CNT diameters of 10 nm and 20 nm, respectively. However, nanocrater catalysts reduce the number of walls from 15 to 5 in 10 nm CNT and from 21 to 11 in 20 nm CNT, compared with pristine catalysts. Fig. 4c, showing CNTs grown vertically from the nanocrater, indicates that whole nanocrater catalysts on the substrate have catalytic activity. Fig. 4d shows the plain view SEM images after removal of some CNTs grown from the substrate; the images show remaining catalysts. These images indicate that the CNTs are formed by bottom-up growth and that the nanocrater catalysts retain their structures during CNT synthesis by MPCVD. In this approach, the exclusive control for the diameter and the number of walls in CNTs is expected to be feasible *via* versatile extension of nanocrater sizes and thicknesses. Therefore, our template-free and sculpting method to synthesize these new crater catalysts may be potentially useful for design of new catalysts and their catalytic properties.

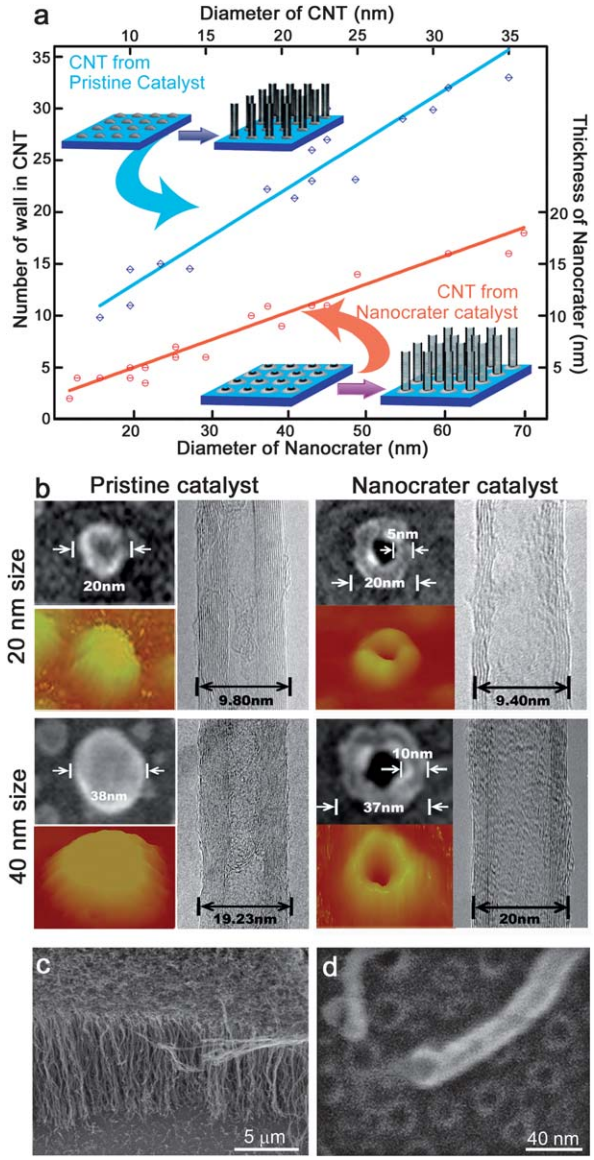

Fig. 4 The catalytic application of nanocraters to exclusively control the diameter as well as the number of walls in the CNT. (a) Plots of the number for walls *versus* diameter for both CNTs from pristine and nanocrater catalysts. Insets are schematic diagrams for CNTs to be grown from pristine and nanocrater catalysts. (b) Representative examples in two different sizes for pristine and nanocrater catalysts (SEM in upper left, AFM in under left) and CNT grown from each catalyst (TEM in upper right, cross-sectional SEM in under right). (c) SEM image of CNTs grown vertically from nanocraters. (d) Plain view SEM images after the removal of some CNTs.

Conclusions

In summary, we have developed the new template-free and sculpting method to allow the exclusive control of the morphologies and structures of nanoparticles in the existing nanoparticle array *via* the simple chemical and plasma processes. Also, their structures and compositions have been clarified by SEM, AFM, and TEM analyses. These results show that the formation of core–shell nanoparticles with the metal core and the oxide shell during the plasma process is the key to the subsequent formation of craters during chemical selective etching. Furthermore, we have demonstrated the use of unique morphologies of nanocrater catalysts as effective templates to simultaneously control the number of walls as well as the outer diameter in a CNT. In this view, these results imply that our template-free and sculpting method to fabricate crater nanoparticles could be further extended to provide the recipe for synthesizing a new class of novel structures.

Acknowledgements

This work was supported by the Korea Center for Artificial Photosynthesis (KCAP) (NRF-2009-C1AAA001-2009-0093879), by the WCU program (R-31-2008-000-10055-0), by the Priority Research Centers Program (NRF-2009-0094039), National Research Foundation (NRF-R0A-2007-000-20029-0), and the Center for Inorganic Photovoltaic Materials (NRF-2010-0007692), and the Hydrogen Energy R&D Center from one of the 21st Century Frontier R&D Programs, and the Secondary Battery Program (NRF-2010-0029042).

Notes and references

1 (*a*) M. T. Tuominen and T. P. Russell, *Science*, 2000, **290**, 2126; (*b*) D. H. Lee, D. O. Shin, W. J. Lee and S. O. Kim, *Adv. Mater.*, 2008,

20, 2480; (*c*) K. M. Choi, S. Augustine, J. H. Choi, J. H. Lee, W. H. Shin, S. H. Yang, J. Y. Lee and J. K. Kang, *Angew. Chem., Int. Ed.*, 2008, **47**, 9904.
2 (*a*) R. Y. Zhang, I. Amlani, J. Baker, J. Tresek, R. K. Tsui and P. Fejes, *Nano Lett.*, 2003, **3**, 731; (*b*) H. Ago, S. Imamura, T. Okazaki, T. Saito, M. Yumura and M. Tsuji, *J. Phys. Chem. B*, 2005, **109**, 10035; (*c*) W. E. Alvarez, F. Pompeo, J. E. Herrera, L. Balzano and D. E. Resasco, *Chem. Mater.*, 2002, **14**, 1853.
3 (*a*) J. Chen, F. Saeki, B. J. Wiley, H. Cang, M. J. Cobb, Z. Y. Li, L. Au, H. Zhang, M. B. Kimmey, X. Li and Y. Xia, *Nano Lett.*, 2005, **5**, 473; (*b*) L. P. Zhu, H. M. Xiao, W. D. Zhang, G. Yang and S. Y. Fu, *Cryst. Growth Des.*, 2008, **8**, 957.
4 (*a*) E. Mathiowitz, J. S. Jacob, Y. S. Jong, G. P. Carino, D. E. Chickering, P. Chaturvedi, C. A. Santos, K. Vijayaraghavan, S. Montgomery, M. Bassett and C. Morrell, *Nature*, 1997, **386**, 410; (*b*) H. Zhang, R. Jin and C. A. Mirkin, *Nano Lett.*, 2004, **4**, 1493.
5 (*a*) J. Dinesh, M. Uzma, P. Mandal and A. Sundaresan, *Angew. Chem.*, 2008, **120**, 7799; (*b*) H. Zeng, W. Cai, P. Liu, X. Xu, H. Zhou, C. Klingshirn and H. Kalt, *ACS Nano*, 2008, **2**, 1661; (*c*) Y. Yin, R. M. Rioux, C. K. Erdonmez, S. Hughes, G. A. Somorjai and A. P. Alivisatos, *Science*, 2004, **304**, 711.
6 C. Colliex, T. Manoubi and C. Ortiz, *Phys. Rev. B: Condens. Matter*, 1991, **44**, 11402.
7 (*a*) J. S. Gao, K. Umeda, K. Uchino, H. Nakashima and K. Muraoka, *Mater. Sci. Eng., B*, 2004, **107**, 113; (*b*) L. Signorini, L. Pasquini, L. Savini, R. Carboni, F. Boscherini, E. Bonetti, A. Giglia, M. Pedio, N. Mahne and S. Nannarone, *Phys. Rev. B: Condens. Matter*, 2003, **68**, 195423.
8 S. L. Semiatin, *Metalworking: Bulk Forming|Prepared Under the Direction of the ASM International Handbook Committee*, ASM International, 2005, vol. 14.
9 (*a*) T. W. Wildoer, L. C. Venema, A. G. Rinzler, R. E. Smalley and C. Dekker, *Nature*, 1998, **391**, 59; (*b*) S. S. Fan, M. G. Chapline, N. R. Franklin, T. W. Tombler, A. M. Cassell and H. J. Dai, *Science*, 1999, **283**, 512; (*c*) A. C. Dillon, K. M. Jones, T. A. Bekkedahl, C. H. Klang, D. S. Bethune and M. J. Heben, *Nature*, 1997, **386**, 377.
10 (*a*) A. Srivastava, O. N. Srivastava, S. Talapatra, R. Vajtai and P. M. Ajayan, *Nat. Mater.*, 2004, **I**, 610; (*b*) L. Delzeit, C. V. Nguyen, B. Chen, R. Stevens, A. Cassell, J. Han and M. Meyyappan, *J. Phys. Chem. B*, 2002, **106**, 5629.

